Molecular Modeling

Cadmium–BINOL Metal–Organic Framework for the Separation of Alcohol Isomers**

Rocio Bueno-Perez, Patrick J. Merkling,* Paula Gómez-Álvarez, and Sofia Calero*[a]

Abstract: The large-scale isolation of specific isomers of amyl alcohols for applications in the chemical, pharmaceutical, and biochemical industries represents a challenging task due to the physicochemical similarities of these structural isomers. The homochiral metal–organic framework cadmium–BINOL (BINOL = 1,1′-bi-2-naphthol) is suitable for the separation of pentanol isomers, combining adsorption selectivities above 5 with adsorption capacities of around 4.5 mol kg^{-1}. Additionally, a slight ability for separation of racemic mixtures of 2-pentanol is also detected. This behavior is explained based on matching shapes, strength of host–guest interactions, and on the network of hydrogen bonds. The last of these explains both the relative success and shortfalls of prediction methods at high loadings (ideal adsorbed solution theory) or at low coverage (separation factors), which are therefore useful here at a qualitative level, but not accurate in quantitative terms. Finally, the high selectivity of cadmium–BINOL for 1-pentanol over its isomers offers prospects for practical applications and some room for optimizing conditions.

Introduction

The group of compounds commonly known as amyl alcohols or pentyl alcohols is composed of 1-pentanol (1P) and seven alcohol structural isomers. Three of these exist in two chiral forms. The commercialized product "amyl alcohol" is a mixture of several of these isomers.[1] These compounds play an important role in industry as organic solvents,[2] but their applications go further. Pentyl alcohols act as intermediates in the production of herbicides and pharmaceuticals, and are also used as additives, flavoring, extraction, and flotation agents.[3] They are frequent byproducts of the chemical, pharmaceutical, and biochemical industries[4] and the large-scale production process is mostly based on halogenation of pentane[2,3,5] or a rhodium-catalyzed hydroformylation and hydrogenation.[2] Given this wide range of production methods, a flexible separation method to obtain higher specific isomers is especially important. The physicochemical similarities of the isomers of pentyl alcohols make the current purification of these compounds by distillation of the alcohol mixtures difficult, and requires numerous unit operations;[2,3,5] a solution that is costly both energetically and economically, and polluting. From this perspective, an alternative method of purification of these isomers might reduce expenses in the production process, reduce the polluting effect on the environment, and generate purer products in less time. In this regard, adsorption-based separation in nanoporous materials represents a relevant option.

Metal–organic frameworks (MOFs) consist of small metal-containing clusters connected three dimensionally by a variety of polydentate ligands,[6] which create open porous structures with high pore volumes and surface areas.[7] The rich design possibilities of MOFs offer a large diversity of chemical compositions and pore dimensions[8] and allow the molecular-sieving properties of MOFs to be extended to larger molecules with a different chemical nature. Recent studies on the adsorption of alcohols in MOFs focused on the design of stable MOFs to extract alcohols from water[9] and for alcohol storage.[9d,e,10] Adsorption mechanisms[9a,11] and flexibility induced by alcohols have also been studied,[9b,d,11,12] but most of these works involve only short-chain alcohols, such as methanol, ethanol, and propanol.

Homochiral MOFs (HMOFs) are a subset of structures from the MOF family. They were first synthesized to perform enantioselective heterogeneous catalysis and study the underlying molecular mechanisms.[13] Similarly to other MOFs, these HMOFs are made up of organic and inorganic building units, although in this case at least one of these building units has to be chiral. Recently, 1,1′-bi-2-naphthol (BINOL)-based ligands have been used to generate the first isoreticular series of HMOFs.[13c,14] Increasing emphasis on chiral drugs and chemicals is fueling the development of new adsorbents for enantio-

[a] R. Bueno-Perez, Prof. Dr. P. J. Merkling, Dr. P. Gómez-Álvarez, Prof. Dr. S. Calero
Department of Physical, Chemical and Natural Systems
Universidad Pablo de Olavide, Ctra. de Utrera, km. 1, 41013 Seville (Spain)
E-mail: pjmerx@upo.es
scalero@upo.es

[**] BINOL = 1,1′-bi-2-naphthol.

Supporting information and the ORCID identification numbers for the authors of this article can be found under http://dx.doi.org/10.1002/chem.201604171.

© 2016 The Authors. Published by Wiley-VCH Verlag GmbH & Co. KGaA. This is an open access article under the terms of the Creative Commons Attribution-NonCommercial License, which permits use, distribution and reproduction in any medium, provided the original work is properly cited and is not used for commercial purposes.

selective separation, and BINOL-based materials have proven to be useful for this type of application.[15]

This study focuses on Cd–BINOL,[13b] a HMOF also known as HMOF-1, due to its distinctive geometry. This MOF is a colorless crystal with the chemical formula $Cd_3L_4(NO_3)_6$, in which L is (*R*)-6,6′-dichloro-2,2′-dihydroxy-1,1′-binaphtyl-4,4′-bipyridine (Figure 1). The space group ($P4_122$) and chiral ligand of this

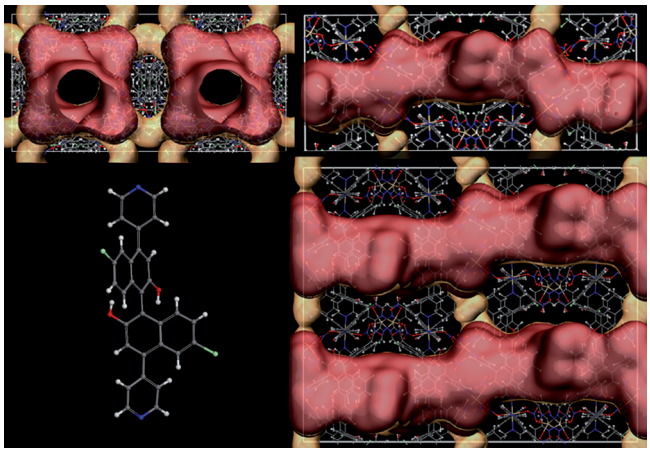

Figure 1. The *xy* view of the channel network inside Cd–BINOL (top-left) and the *zy* view of the network inside the structure (top-right). Chiral bridging ligand (*R*)-6,6′-dichloro-2,2′-dihydroxy-1,1′-binaphtyl-4,4′-bipyridine (bottom-left); the *zx* view of the network inside the structure (bottom-right). In these framework views, the semitransparent red region highlights the main channels, whereas the ochre region signals the side channels. For maximum clarity, a 2×1×1 simulation cell is shown.

structure define helical pores running in the *z* direction connected by zigzag channels running perpendicular to the *z* direction and parallel to the *x* or *y* axes. The analysis and visualization of the accessible void space of the structure reveals the unusual twisted pore shape of the main channel through which a probe of up to 9.25 Å in diameter can diffuse. Likewise, a probe of up to 5.5 Å in diameter can diffuse through the zigzag channels that connect horizontally or vertically with the main channels. As described in Figure S2 in the Supporting Information, the main channels are connected horizontally by their bottom surface with zigzag channels of a total length of 13.5 Å. This pattern is repeated four times along the *z* axis with a rotation of 90°. The aforementioned zigzag channels are referred to as "side channels" hereafter. The areas that can be occupied by molecules that cannot cross these side channels are considered as "windows" with a diameter of 6.5 Å. Thus, Cd–BINOL is characterized by the presence of big pores and unusual pore shapes. This not only ensures a high adsorption capacity, but also suggests possible selective behavior. This study is aimed at investigating the selective adsorption of Cd–BINOL for mixtures of pairs of enantiomers of the chiral molecules 2-pentanol (2P), 2-methylbutanol (2MB), and 3-methyl-2-butanol (3M2B). It also encompasses mixtures involving structural isomers 1P, 2P, 3-pentanol (3P), 2MB, 3-methylbutanol (3MB), 2-methyl-2-butanol (2M2B), 3M2B, and 2,2-dimethylpropanol (22DMP). These molecules are displayed for reference in Figure S1 in the Supporting Information. They are aliphatic alcohol isomers with five carbon atoms that differ in the position of the hydroxyl group, chain structure, or both. We conducted Monte Carlo (MC) simulations at room temperature to compute both single and multicomponent adsorptions that were related to behavior at the molecular level. In particular, apart from thermodynamic analysis, we characterized the host–guest and guest–guest interactions through calculations of populations inside the MOF, radial distribution functions (RDFs), and hydrogen-bonding properties. In addition, we discuss the suitability of ideal adsorbed solution theory (IAST)[16] to predict selectivities and compare them to those obtained at saturation and low-coverage regimes.

Results and Discussion

Separation of optical isomers in Cd–BINOL

Given that Cd–BINOL is a chiral structure, it may well be able to separate chiral mixtures. Therefore, binary mixtures of *R*/*S* enantiomers have been investigated. Three of the pentyl alcohol isomers possess an asymmetric carbon, namely, 2P, 2MB, and 3M2B, whereas the other structural isomers have no asymmetric carbon. Simulations were performed with a racemic mixture as the reservoir. This is expected to be the most challenging separation. It is also the most important and relevant type of separation, on the grounds that most nonenzymatic synthetic routes lead to racemic mixtures. Figure 2 reflects the

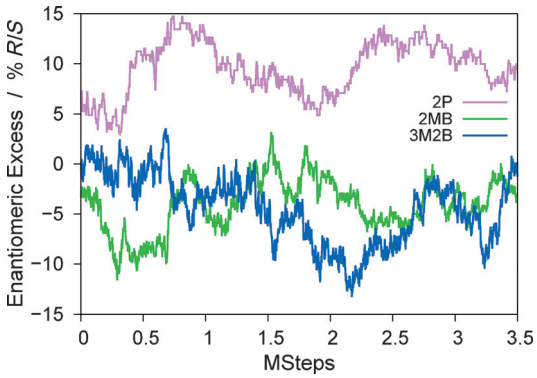

Figure 2. Instantaneous enantiomeric excess (*ee*) of 2P (pink), 2MB (green), and 3M2B (blue) throughout the simulation. The *x* axis indicates the number of MC steps in millions.

evolution of handedness throughout the simulations, averaged over six independent simulations for improved statistics. These simulations were run under conditions of saturation, as specified in the Computational Details section and general results, such as the average number of molecules, can be found in Table 1. The results for the overall handedness are expressed as *ee* values, which, for our purposes, are obtained by using Equation (1):

$$\%ee = 100(x_R - x_S) \quad (1)$$

© 2017 The Authors. Published by Wiley-VCH Verlag GmbH & Co. KGaA, Weinheim

Table 1. Hydrogen-bond statistics for pure compounds in Cd–BINOL at 100 kPa fugacity.[a]

	1P	2P	3P	22DMP
no. simulations	6	6	6	6
N	52.7±0.2	52±0.4	51.2±0.2	41.23±0.11
$N^{\text{side channel}}$	4.04±0.05	3.63±0.17	3.997±0.002	0.000±0.001
f_{1-1}	114±2	117±3	102.1±1.5	113.5±1.8
$f_{1-\text{frwk}}$	14.8±1	13.6±1.4	13.5±0.5	18.5±0.8
$f_{1-1}^{\text{side channel}}$	53±9	37±7	7.4±3.5	–
$f_{1-\text{frwk}}^{\text{side channel}}$	13.5±4.5	24±6	1.2±0.5	–
	2MB	**3MB**	**2M2B**	**3M2B**
no. simulations	6	6	6	6
N	51.7±0.2	50.7±0.6	44.8±0.4	49.2±0.5
$N^{\text{side channel}}$	3.98±0.02	3.86±0.14	0.01±0.004	3.957±0.015
f_{1-1}	110±2	108.4±1.1	108.7±1.6	112±2
$f_{1-\text{frwk}}$	17.6±1.5	20.6±1.2	15.4±0.4	13.9±0.5
$f_{1-1}^{\text{side channel}}$	37±12	26±5	–	15±4
$f_{1-\text{frwk}}^{\text{side channel}}$	30±8	14±3	–	11±3

[a] N is the total number of guest molecules in the unit cell (and simulation box) and $N_{\text{side channel}}$ is the number of guest molecules in the four side channels. All probabilities are given as percentages. The probability of a guest molecule being hydrogen-bonded to other guest molecules is labeled $f_{1\text{-}1}$. The probability of a guest molecule being hydrogen-bonded to atoms of the framework is labeled $f_{1\text{-frwk}}$.

in which x_R and x_S are the mole fractions of *R* and *S* isomers adsorbed, so that the *ee* is a signed value. We expect the system to start in the most favored chiral form and increment that imbalance the longer the simulation goes on, providing the framework is selective towards a chiral form. Changes in chirality do indeed occur spontaneously at this temperature for this force field by inverting like an umbrella. Based on an exponential fit to the autocorrelation function of the handedness (Figure S4 in the Supporting Information), a characteristic correlation length is calculated: its value is four million steps (MSteps) for 2P, and 3 MSteps for 2MB and 3M2B. Given that these lengths are comparable to the lengths of the simulation runs, equilibrium is not reached, but it is still enough for tendencies to emerge. In the (*R/S*)-2MB and (*R/S*)-3M2B mixtures, no separation is found within this level of accuracy. For 2MB, the overall *ee* is −4±4%, whereas for 3 M2B it is −5±4%. On the other hand, 2P slightly favors the *R* enantiomer: the *ee* in this case is 10±4%. With respect to evolution of the curve in the last case, a slight increase in *ee* is observed over the duration of the simulation, as evidenced by the slope of the regression line. On the whole, of all pentyl alcohol isomers, only one pair of stereoisomers presents some degree of separation. For the others, our results show Cd–BINOL to be essentially unfit for the separation of enantiomeric mixtures of either 2MB or 3M2B. This is not to say that Cd–BINOL may not be an interesting material for the separation of some combinations of pentyl alcohols, and thus, the ability of the material to separate structural isomers will be explored next.

Separation of structural isomers in Cd–BINOL

The behavior of eight structural isomers of the general formula $C_5H_{12}O$ is investigated; first, as pure compounds in the Cd–BINOL framework. Figure 3 shows the computed single-component adsorption isotherms for each of these amyl alcohols. Overall, the curves exhibit similar shapes, revealing related adsorption behavior. The onset pressure of adsorption ranges from 0.1 to 10 Pa, approximately, depending on the guest alcohol; it is lowest in 1P and highest in 2M2B. The steep slope of the isotherms provides evidence of rapid pore filling for all adsorbates. A fit of the isotherms by using the Langmuir model increases more slowly, as can be seen in Figure S3 in the Supporting Information. This is because the shape of the isotherms is known as an S curve that the Langmuir model is not able to mimic, and it usually involves some cooperativity to drive the filling.

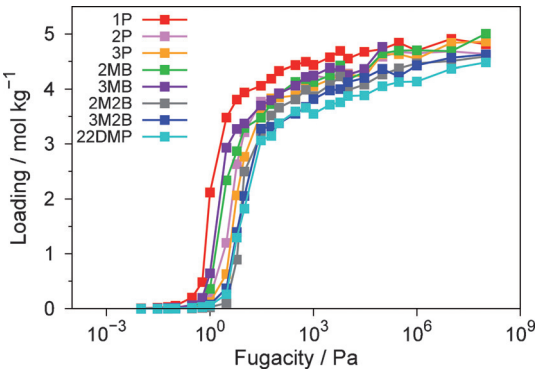

Figure 3. Unary adsorption isotherms of pentanol isomers at 298 K.

Loadings at saturation are between 4 and 5 mol kg^{-1} of adsorbent (about 50 molecules per unit cell). The increasing trend in adsorption capacity correlates loosely with the order of onset of adsorption identified previously. It can also be related to structural features of the alcohol isomers that govern packing ability, that is, increasing level of ramification and position of the hydroxyl group. The interplay between features will be key in the case of competitive adsorption of alcohols in mixtures and shall be examined later in this study.

Low-loading conditions offer an especially interesting perspective for analysis because Henry coefficients used to characterize adsorption behavior relate directly to thermodynamic properties. In contrast to this macroscopic interpretation, from the point of view of intermolecular forces, one might think that adsorption ought to be mediated by the establishment of hydrogen bonds. Figure 4 represents adsorption enthalpy versus the percentage of hydrogen bonds formed between the adsorbate and framework at infinite dilution. Indeed, the more hydrogen bonds formed with the structure, the lower the adsorption enthalpy, and therefore, the stronger the interactions. A linear fit of the data for the different isomers yields an r^2 value of 0.82; a typical value in quantitative structure–activity relationship (QSAR) analysis. Surprisingly, the figures of the percentages of hydrogen bonds formed are very low and

© 2017 The Authors. Published by Wiley-VCH Verlag GmbH & Co. KGaA, Weinheim

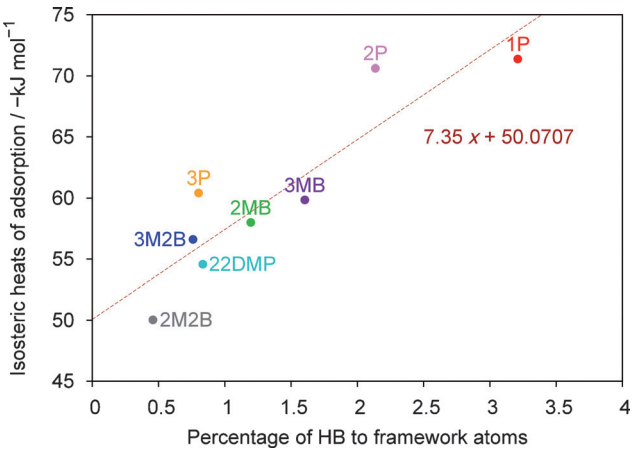

Figure 4. Adsorption enthalpy versus percentage of hydrogen bonds to framework.

cannot account, by themselves, for lowering of the enthalpy. The slope of the linear fit indicates that 735 kJ mol^{-1} would be achieved per hydrogen bond, which is roughly 30 times the enthalpy lowering contribution of the hydrogen bond itself. The overwhelming majority is due to dispersion forces that arise from confinement. In other words, there is correlation with hydrogen bonding, but not causation. Also, extrapolation of the linear fit to zero hydrogen bonds yields a residual enthalpy of −50 kJ mol^{-1}, also due mainly to dispersion interactions. Full thermodynamic data are available in Table S5 in the Supporting Information.

To characterize the favored adsorption sites, the average occupational density profiles at infinite dilution (substance–volume–temperature (NVT) calculations for a single molecule) for all isomers are displayed in Figure 5. They show that molecules tend to occupy three different areas: the main channel, the side channels, and/or the windows to these channels. All isomers occupy the region of the main channel, but only some of them are also located around the windows (3P, 2MB, and 3MB) or within the side channels (1P and 2P). This is not to say that at higher densities side channels cannot be occupied given that this analysis only reveals the behavior at infinite dilution. Figure 5 also highlights that atoms O_5 and O_8 of the framework are located at the windows, whereas atoms Cl_4 and O_{11} are within the channels (atom numbering according to the CIF file).

As the fugacity of the alcohols increases, the framework gradually fills up. To determine the pattern of filling, side-channel occupancy was compared with overall occupancy. This is represented in Figure 6; the *x* axis reports the fraction of molecules adsorbed in the whole structure, taking as a reference a fugacity of 100 kPa, whereas the *y* axis represents the number of molecules adsorbed per side channel. Analyzing the occupancies reveals that a maximum of one amyl alcohol molecule is adsorbed per side channel. The number of molecules per side channel can thus also be interpreted as the fraction of side channels occupied. In this sense, for those amyl alcohols, the curve of which lies above the identity function, side channels fill before the rest of the framework does. This is

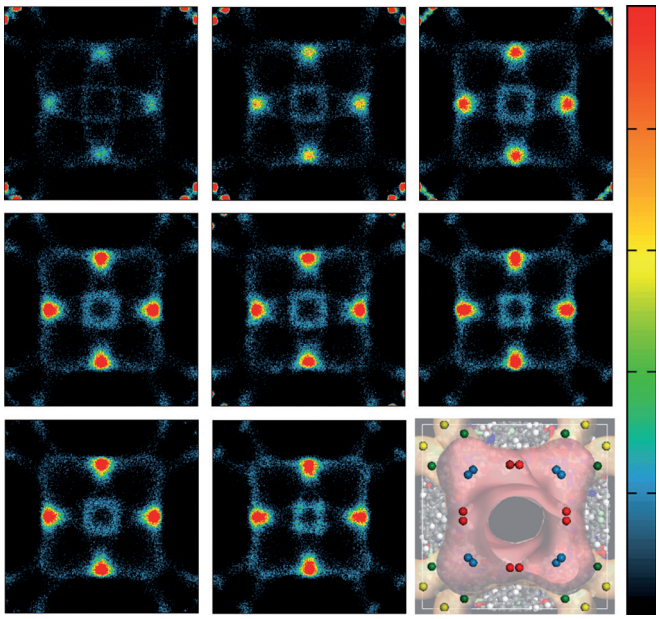

Figure 5. Average occupational density profiles of adsorbate center of mass in an *xy* view. From left to right: 1P, 2P, 3P (top); 2MB, 3MB, 2M2B (middle); 3M2B, 22DMP (bottom) and a representation along the same view that highlights several crucial items of the framework: the location of oxygen atoms O_5, O_8, and O_{11} according to CIF-file notation, belonging to three different nitrate groups, in red, blue, and green, respectively. The yellow spheres mark the center of the side channels.

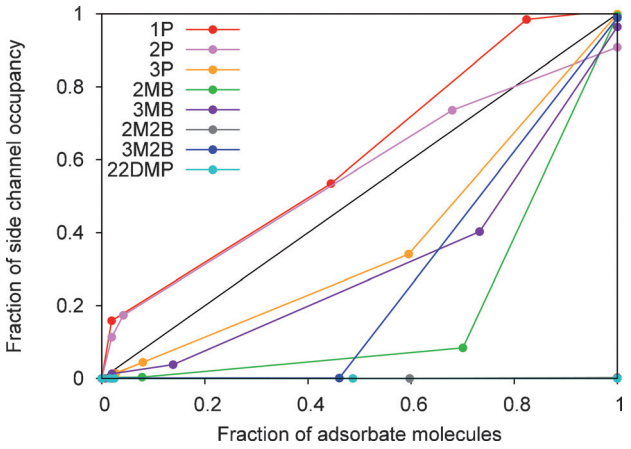

Figure 6. Fraction of side channels occupied versus fraction of total occupancy (referenced to saturation occupancy). The black line graphs the identity function representative of equal affinity for side and main channels.

the case for 1P and 2P. These two isomers had been found previously (Figure 4) to exhibit the highest (in absolute value) heats of adsorption and fraction of hydrogen bonds to the framework, although the calculation included all interactions of the guest molecule with the framework, not just the ones within the side channels. Conversely, isomers 3P, 2MB, 3MB, and 3M2B fill side channels after the rest of the framework does. Finally, the remaining two isomers, 2M2B and 22DMP, do not enter side channels at all. These two isomers share the characteristic of possessing an exceptionally bulky and rigid

© 2017 The Authors. Published by Wiley-VCH Verlag GmbH & Co. KGaA, Weinheim

environment around one of their carbon atoms: based on their heavy-atom skeleton, they are the only isomers in the study that are dibranched on the same carbon atom. As a consequence, they cannot enter narrow channels or pores; this was previously observed in zeolitic imidazolate framework ZIF-77[17].

In the case of isomers that present chirality, namely, 2P, 2MB, and 3M2B, we explored whether handedness was favored in the special confinement conditions of the side channels. The *ee* in the side channels was found to be 26 ± 12 (2P), 4 ± 18 (2MB), and -23 ± 9% (3M2B). Isomer 2MB showed no selective adsorption towards any of the enantiomers, whereas only slightly increased adsorptions were detected in 2P and 3M2B. Based on these results, it does not appear promising to design a separation strategy based on exploiting solely the low-coverage regime in 2P.

After studying the low-coverage regime and the filling behavior with increasing loading, we now turn our attention to the high-loading regime. For pure systems at a fugacity of 100 kPa (close to saturation conditions), Table 1 compiles the results. The hydrogen-bond information in Tables 1–3 is also available as bar charts in the Supporting Information for visual inspection (Figures S5–S7 in the Supporting Information). In Table 1, the percentage of hydrogen bonds between guest molecules is labeled as $f_{1\text{-}1}$. This notation can be straightforwardly extended to pair interactions in binary and ternary mixtures of guest molecules (Tables 2 and 3, respectively, below) and is therefore consistent herein. All isomers maintain, on average, close to four molecules in the four side channels, except 2M2B and 22DMP, as previously noted. The total number of molecules that fit in the framework lies at around 50, except in 2M2B (44.8) and 22DMP (41.2). The difference in the case of 2M2B is satisfactorily explained as a consequence of the empty side channels, whereas in the case of 22DMP packing is also less efficient at this fugacity. As the adsorption isotherm in Figure 3 showed, however, the latter difference gradually vanished at higher fugacities.

The hydrogen-bonding probabilities of the alcohols are similar. Those to other guest molecule $f_{1\text{-}1}$ have values above 100%, typically around 110%. This means that a number of alcohol molecules are involved in more than one hydrogen bond, generally one as a hydrogen-bond donor and one as an acceptor. By taking into account the probability of hydrogen bonding to the framework, the total probability lies at around 125%. A tendency emerges, in which the probabilities are higher in those molecules with more accessible hydroxyl groups, such as in 1P, 2P, or 22DMP, than in less accessible ones, such as 3P, 2M2B, or 3M2B. This effect is small, but significant. Hydrogen bonds form preferably to other guest molecules rather than to the framework. This is a bit surprising, given that the majority of oxygen atoms of the 24 nitrate ions in the framework are accessible (40 out of the 72 atoms) and competing with the alcohol molecules as hydrogen-bond acceptors. Considering only accessible oxygen atoms of the nitrates, and assuming that a hydrogen-bond donor has the same probability of forming a hydrogen bond to a nitrate oxygen atom as that of an alcohol molecule, we would expect $f_{1\text{-frwk}}$ to take values from 25 to 33%. This can also be expressed in a different way. We can define hydrogen-bond selectivity according to Equation (2) in much the same way as adsorption selectivity is defined:

$$S_{\mathrm{HB,\,ij}} = \frac{\frac{n_{\mathrm{HB,i}}}{N_i}}{\frac{n_{\mathrm{HB,j}}}{N_j}} \qquad (2)$$

in which $n_{\mathrm{HB,i}}$ is the number of hydrogen bonds to molecule i and N_i is the number of sites of i (in the case of the framework, it is taken to be the accessible sites). The hydrogen-bond selectivity, $S_{\mathrm{HB,1\text{-}frwk}}$, varies between values of 2.3–2.6 (3MB and 2MB, respectively) and 3.5–3.65 (2P and 3M2B, respectively). Because these values are all well above one, a guest molecule has a stronger affinity to other molecules than to framework sites in terms of hydrogen bonding.

This hydrogen-bond bias towards other guest molecules explains the S-curve behavior of the pure isotherms in Figure 3 observed previously: once guest molecules bind to the framework, other alcohol molecules are easily added due to the preferred formation of alcohol–alcohol hydrogen bonds. The cooperativity occurs in those molecules settled in the framework to draw in further molecules.

In line with the observations made around the results in Figure 6, the inner surface of the side channels is a more hydrophobic environment. All isomers within the side channels form, on average, considerably fewer hydrogen bonds to guest molecules due to confinement, while maintaining comparable probabilities of hydrogen-bond formation to the framework, and as a consequence they form fewer hydrogen bonds per molecule overall. Marked differences can be observed between isomers: especially for 3P, the hydroxyl group of which is buried deep within the channel, which is almost unable to form hydrogen bonds either to the framework or to other guest molecules. The hydroxyl group in 3M2B also lies quite close to the center of mass of the molecule and, as a result, forms fewer hydrogen bonds than the rest of the isomers. This behavior of 3P and 3M2B is also observed at low coverage (Table S6 in the Supporting Information).

The pure adsorption isotherms discussed earlier revealed that 1P was the most easily adsorbed alcohol of those considered herein. Therefore, equimolar binary mixtures of 1P with any other isomer should lead to adsorption isotherms that contain mostly 1P. To check this, to check the ability of Cd–BINOL to separate effectively 1P from mixtures with other pentanol isomers, and to test the ability of IAST to predict adsorption behavior, MC simulations of binary mixtures 1P–2M2B, 1P–3M2B, and 1P–22DMP were conducted. The remaining isomers were also tested against 1P, albeit as part of ternary mixtures. Given that alcohol molecules form many hydrogen bonds with each other, we would expect failure of the IAST model. Nonetheless, these hydrogen bonds already form in the pure compounds that are used as inputs to the model. It is therefore interesting to determine if IAST works and, regardless of the finding, if it can be related to hydrogen-bond networks in the mixtures. Are they a straightforward extension of the hydrogen bonds of pure substances and calculated by applying preset

 © 2017 The Authors. Published by Wiley-VCH Verlag GmbH & Co. KGaA, Weinheim

probabilities? Or, on the contrary, is there a special affinity between different isomers that arises from matching shapes in this confined environment?

The adsorption isotherms of 1P–2M2B, 1P–3M2B, and 1P–22DMP indeed favor strongly 1P at all fugacities (Figure 7). This can be inferred from the MC simulation data, which also show that selectivities are good. However, selectivities are discussed in more detail later. The bulkiest isomers (2M2B and 22DMP) are comparatively the least adsorbed. With respect to IAST predictions, they are qualitatively correct, although serious discrepancies are observed. IAST overestimates the separation capacity for these mixtures. In fact, IAST predicts very similar isotherms for 1P–2M2B and 1P–3M2B, which suggests that 2M2B and 3M2B are adsorbed to the same degree.

The IAST prediction for the binary 2M2B–3M2B mixture even predicts a slight edge for 2M2B, which is contrary to MC simulation results (Figure S9 in the Supporting Information). Also, in the 1P–22DMP mixture, at the higher end of the fugacity range 22DMP would appear to be almost completely excluded according to IAST.

Three ternary mixtures were also studied: 1P–2P–3P, in which the influence of the hydroxyl position was assessed; 1P–2MB–3MB, in which "methylated 1-butanol" was studied with a methyl grafted at carbons 4 (yielding 1P), 3 (3MB), or 2 (2MB); and 2P–2M2B–3M2B, in which methylated 2-butanol was studied with methyl grafted at carbons 4 (2P), 3 (3M2B), or 2 (2M2B). In the equimolar ternary mixture of the linear (in the chemical sense) alcohols, the most adsorbed species is again 1P (the only molecule with a linear heavy-atom backbone in a topological sense), followed by 2P and then 3P (Figure 8). This holds true at all fugacities and the relationship between these three isomers is also roughly maintained throughout the whole fugacity range.

These same observations also hold true in IAST predictions, although IAST overestimates the difference between 1P ad-

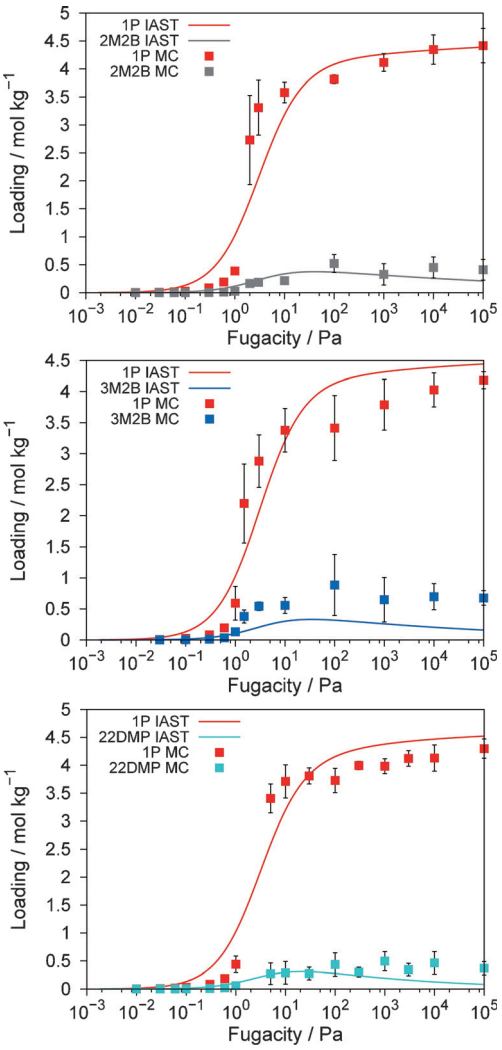

Figure 7. From top to bottom, adsorption isotherms at 298 K of mixtures of 1P–2M2B (red and gray, respectively), 1P–3M2B (red and blue, respectively), and 1P–22DMP (red and turquoise, respectively) obtained by MC simulations (symbols) and predicted by IAST (lines).

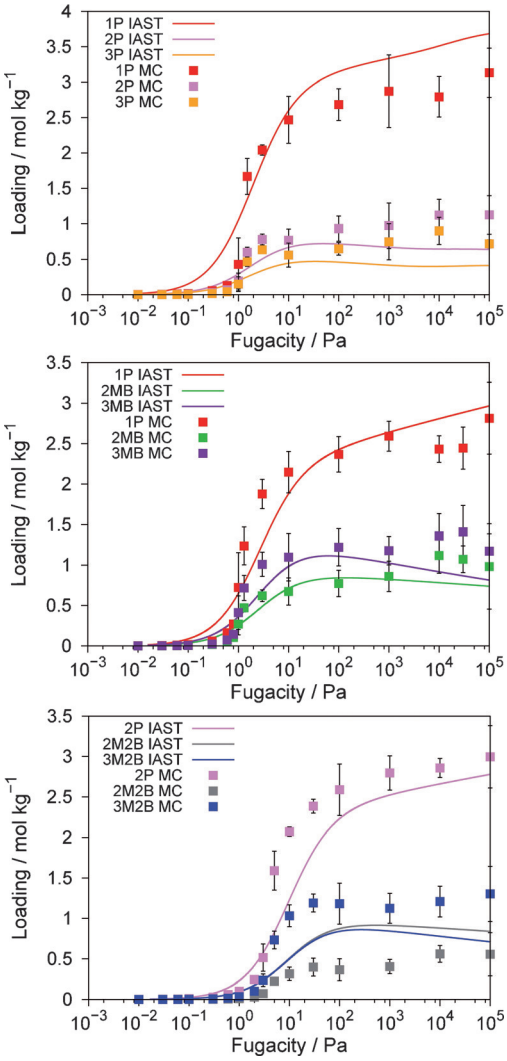

Figure 8. From top to bottom, adsorption isotherms at 298 K of mixtures of 1P–2P–3P (red, magenta, and orange, respectively), 1P–2MB–3MB (red, green, and blue, respectively), and 2P–2M2B–3M2B (magenta, gray, and blue, respectively) obtained by MC simulations (symbols) and predicted by IAST (lines).

© 2017 The Authors. Published by Wiley-VCH Verlag GmbH & Co. KGaA, Weinheim

sorption and any of the other components. The 1P–2MB–3MB mixture leads to very similar conclusions. These compounds are adsorbed in the 1P, 3MB, 2MB order. Two observations can be made: first, the biggest difference is found between linear and branched isomers; and, second, the further away the methyl group, the better for adsorption. These facts are also reflected by IAST predictions in a qualitative way: again, selectivities are overestimated in favor of 1P, whereas the 3MB/2MB selectivity is reproduced fairly well. We now turn to the mixture of 2P–2M2B–3M2B, which, as noted previously, can be formally seen as instances of 2-butanol molecules on which a methyl group has been grafted at positions 4, 2, and 3, respectively, and that is adsorbed in the 2P, 3M2B, 2M2B order. Again, the further away the methyl group, the better for the loading; 3M2B and 2M2B were expected to be similar, even with a slight bias towards 2M2B, which was the least favored guest in the mixture, according to authoritative MC simulations. The reason for this failure of IAST is not due to selective interactions with 2P: in the binary mixture of 3M2B–2M2B, the same mismatch between IAST and MC simulations is observed (Figure S9 in the Supporting Information). To sum up the observations of the adsorption isotherms, the freer the hydroxyl group, the more molecules are adsorbed.

The tendencies observed in isotherms beg the question of whether they can be related to hydrogen-bonding patterns. We therefore had a close look at the statistics of the mixtures, including hydrogen bonding, with an eye to comparing them with the pure compounds. In Table 2, the number of molecules per unit cell is recorded. This number reflects the information given in Figure 8, in which the affinity of the structure for 1P was seen. Table 2 shows that the total number of molecules is higher than that predicted from the number of molecules in the pure systems. This can be quantified as a percentage of excess molecules in the framework, as expressed by Equation (3):

$$\%\mathrm{ads}_{\mathrm{excess}} = \frac{N_{\mathrm{tot}} - \sum x_i N_{i,\mathrm{pure}}}{\sum x_i N_{i,\mathrm{pure}}} \times 100 \qquad (3)$$

Table 2. Hydrogen-bond statistics for binary mixtures.[a]

	1P–2M2B	1P–3M2B	1P–22DMP
no. simulations	12	12	11
N_1	50.0 ± 0.5	44.4 ± 0.5	50.2 ± 0.4
N_2	4.1 ± 0.5	9.7 ± 0.5	3.8 ± 0.3
N_{tot}	54.13 ± 0.15	54.13 ± 0.17	53.9 ± 0.2
$\%\,\mathrm{ads}_{\mathrm{excess}}$	4.2 ± 0.5	3.9 ± 0.6	3.9 ± 0.6
$N_1^{\mathrm{side\ channel}}$	3.997 ± 0.003	3.91 ± 0.07	3.985 ± 0.015
$N_2^{\mathrm{side\ channel}}$	0.000 ± 0.000	0.0005 ± 0.0003	0 ± 0
f_{1-1}	127 ± 2	109 ± 3	126.8 ± 1.4
f_{2-2}	13 ± 3	25 ± 5	9 ± 3
f_{1-2}	11.5 ± 1.5	28.6 ± 1.6	10.5 ± 0.9
f_{2-1}	130 ± 5	129 ± 5	134 ± 4
$f_{1-\mathrm{frwk}}$	16.8 ± 0.7	16.8 ± 0.9	17.1 ± 0.7
$f_{2-\mathrm{frwk}}$	14 ± 3	17 ± 2	14.5 ± 2

[a] Percentages of average self- and cross-association, $f_{i\text{-}i}$ and $f_{i\text{-}j}$, respectively, refer to compound i in the binary mixture. N_i denotes the number of adsorbed molecules of compound i in the mixture. Conditions are at 100 kPa fugacity.

in which x_i is the mole fraction of component i in the adsorbent. This percentage is positive in all cases, and similar among the mixtures studied. Roughly 4% more molecules (in absolute numbers, 2 molecules per unit cell) fit in the porous structure. This fact can be explained because combining molecules of different shapes enables more efficient packing. Although all guest molecules are deformable, their conformational flexibility is not big enough to offset the opportunities for better packing offered by using more than one isomer. Additionally, in those mixtures that contain one of the bulky molecules, 2M2B or 22DMP, that are not able to enter the side channels, excess adsorption will take place because in the mixture the side channels are occupied by the nonbulky isomer, such that there is one molecule in each of the four side channels. This effect is systematic, but small, because it accounts for only 0.6% excess molecules (0.3 excess molecules) in the mixtures of 1P–2M2B and 1P–22DMP.

For the mixture 1P–3M2B, the composition of the side channel is interesting. In this case, each of the adsorbents in the pure state is able to populate the side channels, but in the mixture the side channels only contain 1P. As we established in Figure 6, isomer 1P favors side channels, whereas 3M2B does not and therein lies the explanation.

Table 2 also reveals the percentages of hydrogen bonds formed. For instance, for the first component in the mixture, $f_{1\text{-}1}$ is the percentage of self-association, whereas $f_{1\text{-}2}$ is the percentage of cross-association to the second component. Variable $f_{1\text{-}1}+f_{1\text{-}2}+f_{1\text{-frwk}}$ is the total percentage of hydrogen bonds formed per molecule of the first type, and it is significantly greater than that in single-component adsorptions. Typically, in the mixture, the total percentage is close to 155% and most molecules engage in one hydrogen bond as a donor and one as an acceptor. In fact, $f_{1\text{-}1}$ alone is (in 1P–2M2B and 1P–22DMP) bigger than that in the single-component case. How should we then best think of the arrangement of molecules in the pore? Given that the structure favors markedly 1P and the numbers of molecules of this type in the pure system and the mixtures, we can almost think of the structure as being filled with almost as many 1P molecules as in the single-component case plus a few molecules of different shape. However, the last of these do not merely take advantage of voids in the structure that are unfit for 1P molecules, they completely distort the arrangement within the pores and enhance the average number of hydrogen bonds created. Hydroxyl groups are present in more than one local environment and can adapt better to enable the formation of more hydrogen bonds.

The percentage of hydrogen bonds formed to the framework, on the other hand, remains similar to that of the single-component case. Neither the major nor minor components engage in a significantly greater number of hydrogen bonds to the framework on a per molecule basis, instead they both stay similar. This is slightly counterintuitive because one might think that, given that 1P molecules are already adsorbed at lower fugacities and in greater numbers, they would attach preferably to the framework and pull other ones in, but this is not what happens under these near-saturation conditions. We already alluded to the reason for this behavior in the com-

© 2017 The Authors. Published by Wiley-VCH Verlag GmbH & Co. KGaA, Weinheim

ments on Figure 4: the hydrogen bonds to the framework are not the driving force for adsorption, they represent only a small portion of the interaction enthalpy.

The three ternary mixtures, 1P–2P–3P, 1P–2MB–3MB, and 2P–2M2B–3M2B, previously introduced were analyzed with respect to hydrogen bonding and results are shown in Table 3.

Table 3. Hydrogen-bond statistics for ternary mixtures.[a]

	1P–2P–3P	1P–2MB–3MB	2P–2M2B–3M2B
no. simulations	16	18	18
N_1	33.4 ± 0.5	31.1 ± 0.4	33.9 ± 0.4
N_2	11.9 ± 0.4	10.4 ± 0.3	5.4 ± 0.2
N_3	9.2 ± 0.2	13.1 ± 0.2	14.4 ± 0.3
N_{tot}	54.50 ± 0.16	54.62 ± 0.08	53.72 ± 0.13
% ads_{excess}	4.2 ± 0.5	5.0 ± 0.6	6.3 ± 0.8
$N_1^{side\ channel}$	3.63 ± 0.07	3.90 ± 0.04	3.92 ± 0.05
$N_2^{side\ channel}$	0.32 ± 0.09	0.020 ± 0.009	0.0 ± 0.0
$N_3^{side\ channel}$	0.031 ± 0.008	0.033 ± 0.007	0.002 ± 0.001
f_{1-1}	86 ± 3	78 ± 2	78 ± 2
f_{2-2}	35.2 ± 1.5	31.4 ± 1.5	19.5 ± 1.0
f_{3-3}	28 ± 2	39.0 ± 1.2	48 ± 2
f_{1-2}	31.2 ± 1.5	26.8 ± 0.8	13.8 ± 0.5
f_{2-1}	86 ± 2	79 ± 2	84.9 ± 1.3
f_{1-3}	24.2 ± 1.2	32.7 ± 0.6	38.6 ± 1.0
f_{3-1}	85 ± 2	77.6 ± 1.6	91.7 ± 1.8
f_{2-3}	29.7 ± 1.3	38.3 ± 1.1	45.9 ± 1.6
f_{3-2}	37.8 ± 1.3	30.9 ± 1.3	17.8 ± 0.9
f_{1-frwk}	16.0 ± 0.9	16.4 ± 0.7	16.3 ± 0.5
f_{2-frwk}	14.5 ± 1.1	16.8 ± 0.9	8.8 ± 0.9
f_{3-frwk}	17.5 ± 1.4	16.9 ± 0.7	12.5 ± 0.7

[a] Percentages of average self- and cross-association, f_{i-i} and f_{i-j} ($i \neq j$) respectively, refer to compound i in the ternary mixture. N_i denotes the number of adsorbed molecules of compound i in the mixture.

Again, excess adsorption similar to or larger than that of the binary mixtures is observed. Isomer 1P is the major component, but its share is even larger in the side channels. The only significant minor component in the side channel is 2P, in keeping with observations made around the results reported in Figure 6. Components of the ternary mixtures are involved in many hydrogen bonds on a per molecule basis, comparable to those of the binary mixtures. Hydrogen bonding to the framework is also similar to binary (and pure) systems and similar among components, regardless of them being major or minor components of the mixture. One noticeable exception is the unusually low hydrogen-bonding probability of 2M2B to the framework in the last mixture. A possible explanation for this is that 2M2B is less prone to form hydrogen bonds to the framework at low coverage (Figure 4), and, although at saturation it ultimately does, it is probably less competitive than the rest of the isomers in the mixture. All in all, the findings for the ternary mixtures are similar to those of the binary mixtures.

To refine the analysis and answer the question whether there is a special affinity for hydrogen bonds of a given type, for instance, self- or cross-association, we must take into account the number of molecules of each type within the adsorbent. This can be done by comparing the percentages to those from a probabilistic model fitted to reproduce the total association of every component. Details are described and discussed in the Supporting Information and results are presented in Tables S7 and S8. The most important conclusions are that all components of the mixture engage in more hydrogen bonds than their pure counterpart system, especially the minor components. Although the distribution is roughly random, significant deviations occur. Self-association is favored over cross-association. In ternary mixtures, the cross-association between the two minor components of the mixture also appears to be comparatively favored.

The analysis of pure isotherms or the IAST method generally work well to single out the minor components of a mixture, but the numbers for these minor components in the MC simulations are boosted by the fact that they are able to occupy suitable local environments in the structure in which they can establish more hydrogen bonds on average. This is because the higher adsorbate loading in the mixtures makes hydrogen bonds less prone to break.

Hydrogen bonds thus have an influence on the capacity of IAST results to predict satisfactorily the results of the much more time consuming (but more reliable) MC simulations. In Table S9 in the Supporting Information, qualitative IAST performance is matched against a qualitative assessment of hydrogen-bonding abnormalities based on quantitative criteria. Overall, the qualitative agreement is satisfactory: there are eight coincidences, three tests are inconclusive, and there is one failure.

The previous conclusions reached by introducing the probabilistic model could also have been derived, or at least suspected, from the analysis of RDFs (also known as $g(r)$ functions), such as those shown in Figure 9. Nevertheless, this is a less reliable procedure because the RDFs graph oxygen–oxygen distributions, but not hydrogen bonds directly. Of those oxygen pairs within a suitable distance for hydrogen bonding, roughly 10% are not actually engaged in hydrogen bonding. Figure 9 shows as a representative case the 1P–1P RDF of the pure system and compares it with several oxygen–oxygen RDFs taken from the 1P–2P–3P mixture. The RDF for the oxygen atoms in the single 1P adsorbate system has

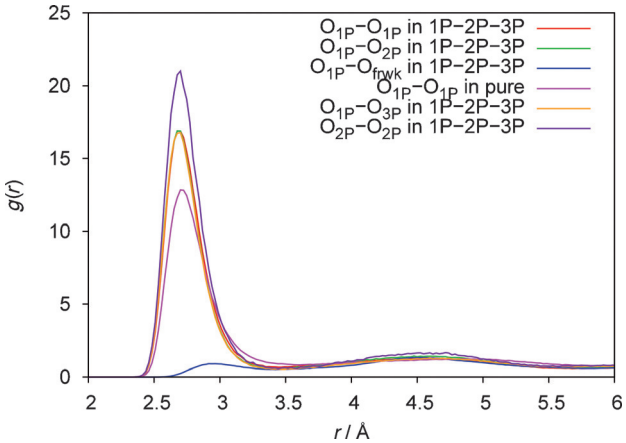

Figure 9. Oxygen–oxygen RDFs at saturation, in a ternary mixture of 1P–2P–3P: O_{1P}–O_{1P}, O_{1P}–O_{2P}, O_{1P}–O_{3P}, O_{1P}–O_{frwk}, O_{2P}–O_{2P}, and pure O_{1P}–O_{1P}.

© 2017 The Authors. Published by Wiley-VCH Verlag GmbH & Co. KGaA, Weinheim

a peak value of 12.8, whereas 1P oxygen involved in ternary mixtures of 1P–2P–3P has a considerably higher peak value if measured against 1P, 2P, or 3P, as a consequence of 1P engaging generally in more hydrogen bonds in the mixture. The O_{2P}–O_{2P} peak in this mixture is also displayed; it is in fact the highest peak in the graph and highlights increased self-association over cross-association. The distance distribution of O_{1P} to the oxygen atoms of the framework has a local first maximum of 0.9, which highlights weak interactions with the framework, but RDFs also provide new information. In the mixture, peaks are slightly shifted towards smaller distances.

The effect is small, but is a consequence of the higher number of molecules found in the mixtures relative to pure adsorbates. This is also the reason why RDFs of the mixture are slightly less broad. The second maximum in the RDFs has a value in the range 1.3–1.6 and is located at around 4.60 Å (versus values of 0.85–1.2 in the pure compounds and shifted 0.05–0.30 Å), and the third is generally barely noticeable. In the pure substances, this second maximum is lower. This shows that the order within the pores increases in the mixtures.

Adsorption isotherms in pure systems and mixtures thereof have been considered so far and rationalized. Likewise, we examine these data more specifically from the important point of view of adsorption selectivity. Although we are mainly interested in selectivity at high loadings, which would be the ones of most practical interest, we are also keen on assessing the suitability of the calculations of this magnitude at low coverage from the ratio of Henry coefficients to predict the values at finite pressure. These values can be calculated quite quickly, and we therefore compare them with IAST selectivity stemming from our previous calculations.

The ratio of Henry coefficients of pure components has been demonstrated to be a very useful approximation of selectivity at low loading.[18] Pore type and size of the adsorbent and molecular weight and shape of the adsorbate have a profound effect on enthalpy and entropy, which determine the Henry coefficients.[19] Thus, Henry coefficients reflect the adsorption equilibrium at low coverage and the interaction of molecules with the strongest adsorption sites.[20] The selective potential of an adsorbent can be determined through the separation factor (α_{ij}), which expresses the over- or under-representation of component i over j in the adsorbent and is calculated as the ratio of the Henry coefficients for these compounds [K_{hi} and K_{hj}; Eq. (4)].

$$\alpha_{ij} = \frac{K_{hi}}{K_{hj}} \tag{4}$$

The separation factor corresponds to the adsorption selectivity calculated for the low-coverage regime. To evaluate the accuracy and reliability of this separation factor, adsorption selectivity (S_{ij}) is also calculated through the ratio of adsorption loadings, N_i and N_j, of components i and j in the mixture at a fugacity of 100 kPa [Eq. (5)].

$$S_{ij} = \frac{N_i}{N_j} \tag{5}$$

Figure 10 provides a comparison of the values of separation factor and selectivity. The pairs of compounds are those involved in the equimolar mixtures studied through the analysis of adsorption, as shown in Figures 7 and 8 and Figures S8–S10 in the Supporting Information. In general terms, separation factors overestimate selectivity by up to a factor of two. Underestimation, on the contrary, is not frequent and, when it happens, it is only small. As mentioned previously, Henry coefficients reveal the adsorption equilibrium at low coverage and the separation factor that explains selectivity considers only host–guest interactions. The selectivity calculated from adsorption loadings at finite fugacity (100 kPa), on the contrary, is influenced by host–guest and guest–guest interactions. Thus, especially in systems with low guest–guest interactions, the match between separation factor and adsorption selectivity is expected to be good. Clearly, this is not the case for the pentanol isomers in this study, but selectivity is a competition and, if guest–guest interactions affect the components similarly, these selectivities can still be rather similar due to error compensation. Taking into account the crudeness of the approach for these models, it is indeed surprising that extrapolation of the adsorption selectivity from infinite dilution is quite good. In fact, a linear regression yields a better correlation factor than

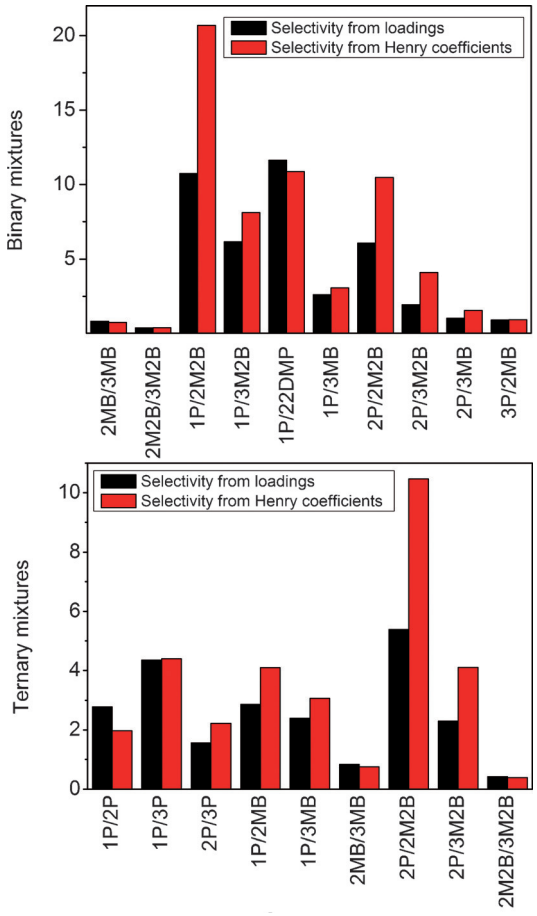

Figure 10. Adsorption selectivity calculated through adsorption loadings (black) and Henry coefficients (red) for several components of bi- (top) and ternary (bottom) mixtures.

© 2017 The Authors. Published by Wiley-VCH Verlag GmbH & Co. KGaA, Weinheim

that of IAST to the MC adsorption selectivity. In short, adsorption selectivity can be predicted both by the separation factor and by IAST; it is crudely similar to those obtained from MC simulations, although generally too optimistic for altogether different reasons.

On the other hand, looking exclusively at adsorption selectivity, there are some pairs that show values over five at high loading, which means adsorption in the structure of the first compound, whereas the second compound is largely excluded. The fact that this is achieved in an adsorbent with big pores, at high loading, is important because it enables fast separation of great amounts of matter without clogging up the structure. Generally speaking, some combinations of adsorbent and mixtures of adsorbates are known to achieve impressive values of selectivity at low loading,[21] but at higher loading these selectivities decrease considerably, which makes the adsorbent of less practical value. Cd–BINOL strongly favors 1P over 2M2B, 3M2B, and 22DMP. As explained before, 1P is an unbranched isomer and 2M2B, 3M2B, and 22DMP are the bulkiest isomers, the structural features of which shield the functional group. The three-dimensional shape of the rest of the compounds in the group of alcohol isomers, 2P, 3P, 2MB, and 3MB, are intermediate between 1P and the 2M2B/3M2B/22DMP group, and their separation from each other is more difficult.

Conclusions

The adsorption of pentanol isomers and mixtures thereof has been studied in Cd–BINOL. This chiral structure adsorbs slightly more (*R*)-2P than the *S* isomer from a racemic mixture.

Results at low coverage indicate that only the linear (1P) or closest to linear (2P) isomers are found in the side channels of the structure preferably to the main channels. Two of the isomers, 2M2B and 22DMP, do not enter the side channels at all up to the fugacity probed (100 kPa).

At higher values of fugacity, adsorption of linear 1P is favored over branched molecules. As a general rule, adsorption is most favored the further away the bulkiest part of the molecule is from the hydroxyl group. Therefore, isomer 1P is clearly favored over 3MB and this, in turn, is slightly favored over 2MB. This also indicates that isomers that share similar structural features are difficult to separate by using this framework. This is the case for 3MB, 3P, and 2MB.

Adsorption selectivities at low coverage, that is, separation factors, recorded values up to 20 and did not drop too strongly, at most by a factor of two and only for the highest values, when fugacity increased to 100 kPa. It follows that separation factors could have been used to predict selectivities at higher fugacities: they prove reliable in their tendencies, although not accurate. The selective behavior is generally overestimated. Alternative predictions through the IAST method reproduce mixture isotherms qualitatively. Despite accounting implicitly for some guest–guest interactions, overall selectivity predictions do not improve. As a quantitative predictive tool, IAST is therefore not fit for purpose in these systems.

To find out the reasons for the behavior of IAST, hydrogen bonds were analyzed. For the pure substances, all isomers engage in similar numbers of hydrogen bonds, around 1.25 per molecule, of which an unexpectedly low 0.15 correspond to bonds to the framework. In mixtures containing 1P, the total number of hydrogen bonds rises to around 1.55 for the major component 1P, and the total number of molecules in the framework increases by 4%. As a consequence, the order increases, as manifested by oxygen–oxygen $g(r)$ functions. The number of hydrogen bonds to the framework remains similar to the pure case, both for major and minor components. Side channels are occupied almost exclusively by 1P (or in its absence by 2P). All components of the mixture engage in more hydrogen bonds than their pure counterpart system, especially the minor components. Furthermore, self-association is found to be slightly favored over cross-association. Qualitative IAST performance is matched against a qualitative assessment of hydrogen-bonding abnormalities based on quantitative criteria to yield satisfactory agreement.

The picture that emerges for these mixtures is a departure from the major component network. Minor components are instrumental in increasing the packing due to shape complementarity and increased hydrogen bonding. Hydroxyl groups in a multicomponent system are present in more than one local environment and can adapt better to enable the formation of more hydrogen bonds.

Finally, and keeping in mind possible applications for purification, we have found that Cd–BINOL behaves selectively towards 1P at saturation, notwithstanding the large size of the main channel. This is promising because this structure achieves a high loading under these conditions that should enable fast separation. Overall, this MOF thus appears as a promising candidate for adsorption-based separations of mixtures of alcohol isomers, providing a low-energy separation alternative to current technologies.

Computational Details

Models and force fields

The Cd–BINOL structure was taken from crystallographic information in the literature[13b] and is compiled in Table S1 in the Supporting Information. In the discussion throughout this work, the atom numbering followed the crystallographic CIF file: thus, there were four crystallographically distinct oxygen atoms on the naphthols (O_1–O_2 and O_3–O_4 on ligands 1 and 2, respectively), nine oxygen atoms in three nitrate ions (O_5–O_7, O_8–O_{10}, and O_{11}–O_{13}), and chlorine on the naphthols (Cl_1–Cl_2 and Cl_3–Cl_4 on ligands 1 and 2, respectively). The pyridine N atoms were coordinated to Cd, and thus, not accessible. To gain a better insight into the accessible space inside the structure and the shape and size of its channels, probes of different diameter sizes were moved along the channels by using Pore Blazer software.[22] This software considered the van der Waals radii of framework atoms and checked the connectivity of channels by using probes of a given diameter. Thus, a detailed view of the accessible space was available and analyzed.

Given that no validated flexible force field has yet been developed, it was a safer approach to keep the framework rigid throughout the simulations. Most of the accessible area available to the guests stemmed from a ligand containing fused aromatic rings that were very rigid, and merely binding of the ligand to the framework

© 2017 The Authors. Published by Wiley-VCH Verlag GmbH & Co. KGaA, Weinheim

metal cations could allow for structural low-frequency deformations. The computer resources saved in this way were available for improving the statistics of the runs. The host–guest and guest–guest interactions were defined through both Lennard–Jones (L-J) and Coulombic potentials. Cd–BINOL was modeled by using the L-J parameters from UFF[23] and the charges described previously[15a] (Table S2 in the Supporting Information). The alcohol adsorbates were flexible and based on L-J parameters; charges (Table S3 in the Supporting Information) and geometries were defined by the TraPPE force field,[24] with flexible bonds (Table S4 in the Supporting Information). The L-J cross interactions were calculated according to Lorentz–Berthelot mixing rules.

Simulation details

Adsorption isotherms of the target alcohols for both single components and mixtures were computed at 298 K with RASPA software[25] by using grand canonical MC (GCMC) simulations. In this ensemble, the chemical potential, volume, and temperature were kept fixed (μVT). The chemical potential (μ) was related to the imposed fugacity. A $1\times1\times1$ unit cell was chosen and, given that the L-J cutoff radius was set to 10 Å, all dimensions of the simulation box were larger than twice the cutoff radius. Periodic boundary conditions[26] were applied. Long-range electrostatic interactions were evaluated by using the Ewald summation technique. Simulations were arranged in cycles of trial moves, including configurational-biased insertions, deletions, and total and partial reinsertions, as well as random translations and rotations of the molecules. In the case of mixtures, simulations could be speeded up by introducing an additional energy-biased identity change move with the same probability as other intended moves. Each point of the isotherm was obtained after 4×10^6 cycles.

Six independent MC μVT simulations at 10^5 Pa were carried out in systems of a single adsorbate species, whereas 12 simulations were launched per binary mixture and 18 for each ternary mixture. In the case of chiral compounds, a racemic bulk composition was chosen. All errors given in the tables and figures herein were standard deviations of the mean. After 10^5 cycles of initialization, simulations comprised 4×10^6 cycles of production. The number of adsorbate molecules in the system was monitored throughout the simulations and so was their average over the independent simulations, and analyzed as a function of production time. An increase of typically around one adsorbate molecule was observed in the systems of both pure adsorbates and mixtures thereof throughout the first 500 000 cycles. This sequence of the simulation had therefore to be reassigned to initialization time and production was only considered from that point on. Following this procedure, calculations of the excess number of adsorbents in mixtures maintained the errors within reasonable boundaries for a statistically meaningful analysis.

Configurations from simulations at saturation taken every 1000 cycles were used to determine valuable microscopic information, such as chirality of the adsorbates, side-channel occupancy, and average hydrogen-bonding properties of the systems.

Hydrogen-bond analysis relied on a well-established set of geometric criteria for hydrogen bonds:[27] O–O distance less than 3.5 Å, intermolecular O–H distance below 2.6 Å, and H–O_{intra}–O_{inter} angle below 30°. No distinction was made between hydrogen-bond donors and acceptors. Alcohols were considered to be within one of the four side channels (or zigzag pores) of Cd–BINOL if their center of mass was within 4 Å of the geometrical center of the O_{11}–O_{11}–Cl_4–Cl_4 moiety (atom indices were according to the CIF file).[13b] Chirality was determined by the sign of the chiral volume (obtained by calculating the scalar triple product). TraPPE models carbon centers as united atoms, and therefore, the sign of the chiral volume revealed the handedness of the center.

Complementary simulations in the canonical ensemble (NVT) were also conducted at 298 K for a single molecule, together with simulations in the grand canonical ensemble at 1 and 10 Pa, and at saturation (10^5 Pa) to compute density profiles (single-molecule simulations) and RDFs (at saturation) and hydrogen bonding with framework atoms (single-molecule simulations and at saturation). Henry coefficients, enthalpies, and entropies were obtained by using the Widom Test Particle insertion method.[26] In the canonical ensemble (NVT), random moves involved molecular translation, rotation, and reinsertion.

The adsorption isotherms of the considered mixtures were also predicted by using IAST[16] from results of the pure components. In the IAST methodology, the adsorption isotherm of each compound could be integrated from either experimental or calculated data of the pure adsorbates and fitted to an isotherm model. Herein, the adsorption isotherm for each compound was obtained by MC simulations. The following isotherm models were probed: Toth,[28] Jensen,[29] Langmuir–Freundlich dual site,[30] Janovic,[31] and Langmuir.[32] None of them outperformed the others in reproducing the data, so pure isotherms were fitted by using the Langmuir model (Figure S3 in the Supporting Information), which was the simplest, best-established model available able to reproduce the computed adsorption isotherms reasonably well. An added benefit of this model was that the fitting procedure was very robust.

All mixtures discussed herein maintained equimolar amounts in the reservoir and, depending on the affinity of the components for the adsorbent, this translated into different numbers of molecules or mole fractions within the adsorbent structure. Both bi- and ternary mixtures of isomers were examined, but this was not set up as a systematic study aimed at exhausting all possible combinations. Rather, mixtures comprised isomers related by some common structural feature or modification thereof. We also explored the relative adsorption of two components in ternary mixtures versus their adsorption in binary mixtures by using IAST methodology and MC simulations. In this way, the 2MB–3MB mixture was compared directly and in combination with 1P, and all three pairwise combinations of 2P–2M2B–3M2B were compared with the ternary mixture. In all cases and methodologies, not only was the qualitative behavior the same, but the ratio of adsorbed molecules was also similar within the error bars of the technique.

Acknowledgements

This work is supported by the European Research Council through an ERC Starting Grant (ERC2011-StG-279520-RASPA), by MINECO (CTQ2013-48396-P), and by the Andalucía Region (FQM-1851).

Keywords: adsorption · alcohols · enantioselectivity · metal–organic frameworks · molecular modeling

[1] R. E. Gosselin, R. P. Smith, H. C. Hodge, J. E. Braddock, *Clinical Toxicology of Commercial Products*, 5th ed., Williams & Wilkins, Baltimore, **1994**.

[2] F. Ullmann, W. Gerhartz, Y. S. Yamamoto, F. T. Campbell, R. Pfefferkorn, J. F. Rounsaville, in *Ullmann's Encyclopedia of Industrial Chemistry*, 7th ed., Wiley-VCH, Weinheim, **2011**.

[3] a) E. Browning, D. R. Buhler, D. J. Reed, *Toxicity and Mechanisms of Industrial Solvents*, 2nd ed., Elsevier, Amsterdam, **1989**; b) M. J. O'Neil, in T *he*

 © 2017 The Authors. Published by Wiley-VCH Verlag GmbH & Co. KGaA, Weinheim

Merck Index: An Encyclopedia of Chemical, Drugs and Biologicals, 14th ed., RSC, Cambridge, **2006**.
[4] E. P. Ivanova, M. A. Kostova, B. K. Koumanova, *Asia-Pac. J. Chem. Eng.* **2010**, *5*, 869 – 881.
[5] a) R. J. Lewis, Jr., *Hawley's Condensed Chemical Dictionary*, Wiley, Hoboken, **2002**; b) J. I. Kroschwitz, A. Seidel, in *Kirk-Othmer Encyclopedia of Chemical Technology*, 5th ed., Wiley, Hoboken, **2006**.
[6] a) B. L. Chen, M. Eddaoudi, S. T. Hyde, M. O'Keeffe, O. M. Yaghi, *Science* **2001**, *291*, 1021 – 1023; b) A. K. Cheetham, C. N. R. Rao, *Science* **2007**, *318*, 58 – 59; c) J. L. C. Rowsell, E. C. Spencer, J. Eckert, J. A. K. Howard, O. M. Yaghi, *Science* **2005**, *309*, 1350 – 1354; d) X. B. Zhao, B. Xiao, A. J. Fletcher, K. M. Thomas, D. Bradshaw, M. J. Rosseinsky, *Science* **2004**, *306*, 1012 – 1015; e) M. Eddaoudi, J. Kim, N. Rosi, D. Vodak, J. Wachter, M. O'Keeffe, O. M. Yaghi, *Science* **2002**, *295*, 469 – 472; f) H. Li, M. Eddaoudi, M. O'Keeffe, O. M. Yaghi, *Nature* **1999**, *402*, 276 – 279.
[7] D. Jiang, A. Urakawa, M. Yulikov, T. Mallat, G. Jeschke, A. Baiker, *Chem. Eur. J.* **2009**, *15*, 12255 – 12262.
[8] a) S. Kitagawa, R. Kitaura, S. Noro, *Angew. Chem. Int. Ed.* **2004**, *43*, 2334 – 2375; *Angew. Chem.* **2004**, *116*, 2388 – 2430; b) G. Férey, *Chem. Soc. Rev.* **2008**, *37*, 191 – 214; c) S. Kitagawa, R. Matsuda, *Coord. Chem. Rev.* **2007**, *251*, 2490 – 2509.
[9] a) A. Nalaparaju, X. S. Zhao, J. W. Jiang, *J. Phys. Chem. C* **2010**, *114*, 11542 – 11550; b) X.-L. Liu, Y.-S. Li, G.-Q. Zhu, Y.-J. Ban, L.-Y. Xu, W.-S. Yang, *Angew. Chem. Int. Ed.* **2011**, *50*, 10636 – 10639; *Angew. Chem.* **2011**, *123*, 10824 – 10827; c) T. Borjigin, F. Sun, J. Zhang, K. Cai, H. Ren, G. Zhu, *Chem. Commun.* **2012**, *48*, 7613 – 7615; d) K. Inumaru, T. Kikudome, H. Fukuoka, S. Yamanaka, *J. Am. Chem. Soc.* **2008**, *130*, 10038; e) Y. F. Chen, J. Y. Lee, R. Babarao, J. Li, J. W. Jiang, *J. Phys. Chem. C* **2010**, *114*, 6602 – 6609.
[10] H. Li, W. Shi, K. Zhao, Z. Niu, X. Chen, P. Cheng, *Chem. Eur. J.* **2012**, *18*, 5715 – 5723.
[11] K. Uemura, Y. Yamasaki, F. Onishi, H. Kita, M. Ebihara, *Inorg. Chem.* **2010**, *49*, 10133 – 10143.
[12] R. I. Walton, A. S. Munn, N. Guillou, F. Millange, *Chem. Eur. J.* **2011**, *17*, 7069 – 7079.
[13] a) C. D. Wu, A. Hu, L. Zhang, W. B. Lin, *J. Am. Chem. Soc.* **2005**, *127*, 8940 – 8941; b) C.-D. Wu, W. Lin, *Angew. Chem. Int. Ed.* **2007**, *46*, 1075 – 1078; *Angew. Chem.* **2007**, *119*, 1093 – 1096; c) K. Gedrich, M. Heitbaum, A. Notzon, I. Senkovska, R. Froehlich, J. Getzschmann, U. Mueller, F. Glorius, S. Kaskel, *Chem. Eur. J.* **2011**, *17*, 2099 – 2106.
[14] L. Ma, J. M. Falkowski, C. Abney, W. Lin, *Nat. Chem.* **2010**, *2*, 838 – 846.
[15] a) X. Bao, L. J. Broadbelt, R. Q. Snurr, *Mol. Simul.* **2009**, *35*, 50 – 59; b) K. Suh, M. P. Yutkin, D. N. Dybtsev, V. P. Fedin, K. Kim, *Chem. Commun.* **2012**, *48*, 513 – 515; c) P. Z. Moghadam, T. Dueren, *J. Phys. Chem. C* **2012**, *116*, 20874 – 20881.
[16] A. L. Myers, J. M. Prausnitz, *AIChE J.* **1965**, *11*, 121.
[17] R. Bueno-Perez, J. J. Gutierrez-Sevillano, D. Dubbeldam, P. J. Merkling, S. Calero, *ChemPhysChem* **2015**, *16*, 2735.
[18] a) D. M. Ruthven, *Principles of Adsorption and Adsorption Processes*, Wiley-Interscience, New York, **1984**; b) T. Duerinck, R. Bueno-Perez, F. Vermoortele, D. E. D. Vos, S. Calero, G. V. Baron, J. F. M. Denayer, *J. Phys. Chem. C* **2013**, *117*, 12567.
[19] a) J. F. Denayer, G. V. Baron, *Adsorption* **1997**, *3*, 251; b) R. A. Ocakoglu, J. F. Denayer, G. B. Marin, J. A. Martens, G. V. Baron, *J. Phys. Chem. B* **2003**, *107*, 398.
[20] J. F. Denayer, G. V. Baron, G. Vanbutsele, P. A. Jacobs, J. A. Martens, *Chem. Eng. Sci.* **1999**, *54*, 3553.
[21] D. Dubbeldam, R. Krishna, S. Calero, A. Ö. Yazaydin, *Angew. Chem. Int. Ed.* **2012**, *51*, 11867 – 11871; *Angew. Chem.* **2012**, *124*, 12037 – 12041.
[22] L. Sarkisov, A. Harrison, *Mol. Simul.* **2011**, *37*, 1248 – 1257.
[23] A. K. Rappe, C. J. Casewit, K. S. Colwell, W. A. Goddard, W. M. Skiff, *J. Am. Chem. Soc.* **1992**, *114*, 10024 – 10035.
[24] a) B. Chen, J. J. Potoff, J. I. Siepmann, *J. Phys. Chem. B* **2001**, *105*, 3093 – 3104; b) M. S. Kelkar, J. L. Rafferty, E. J. Maginn, J. I. Siepmann, *Fluid Phase Equilib.* **2007**, *260*, 218 – 231.
[25] D. Dubbeldam, S. Calero, D. E. Ellis, R. Q. Snurr, RASPA Version 1.0 ed., Northwestern University, Evanston, IL, **2008**.
[26] D. Frenkel, B. Smit, *Understanding Molecular Simulations. From Algorithms to Applications*, Elsevier, Amsterdam, **2002**.
[27] M. Haughney, M. Ferrario, I. R. McDonald, *J. Phys. Chem.* **1987**, *91*, 4934 – 4940.
[28] J. Toth, *Acta Chim. Acad. Sci. Hung.* **1962**, 15, 415 – 430.
[29] C. R. C. Jensen, N. A. Seaton, *Langmuir* **1996**, *12*, 2866 – 2867.
[30] R. Sips, *J. Phys. Chem.* **1948**, *16*, 490 – 495.
[31] D. S. Jovanovic, *Kolloid Z. Z. Polym.* **1969**, *235*, 1203 – 1213.
[32] I. Langmuir, *J. Am. Chem. Soc.* **1918**, *40*, 1361 – 1368.

Manuscript received: September 2, 2016
Accepted Article published: November 8, 2016
Final Article published: December 8, 2016

 © 2017 The Authors. Published by Wiley-VCH Verlag GmbH & Co. KGaA, Weinheim